

# Melting Behaviors of Icosahedral Metal Clusters Studied by Monte Carlo Simulations

YOUNG JOO LEE,<sup>1</sup> JAE YEOL MAENG,<sup>1</sup> EOK-KYUN LEE,<sup>1</sup>  
BONGSOO KIM,<sup>1</sup> SEHUN KIM,<sup>1</sup> KYU-KWANG HAN<sup>2</sup>

<sup>1</sup>*Department of Chemistry and Center for Molecular Science, Korea Advanced Institute of Science and Technology, Taejeon, Korea*

<sup>2</sup>*Department of Physics, Paichai University, Taejeon, Korea*

*Received 9 August 1999; accepted 1 November 1999*

**ABSTRACT:** We present an atom-resolved analysis method that traces physical quantities such as the root-mean-square bond length fluctuation and coordination number for individual atoms as functions of temperature or time. This method is applied to explain the temperature-dependent behaviors of three types of Ni<sub>N</sub> (*N* = 12, 13, 14) clusters. The detailed studies for the three types of clusters reveal characteristics as follows: (a) as the temperature increases, all three types of clusters undergo two-stage melting, irrespective of the existence of vacancy or adatom on the icosahedral surfaces, (b) the melting of icosahedral clusters with vacancy starts with vacancy hopping, which has not been observed for any type of small clusters (*N* < 34), (c) the melting of the icosahedral clusters with adatom (*N* = 14) is initiated by adatom hopping, followed by the site exchange between the adatom and surface atoms. © 2000 John Wiley & Sons, Inc. *J Comput Chem* 21: 380–387, 2000

**Keywords:** Monte Carlo simulation; transition metal clusters; melting; second moment approximation; icosahedron

*Correspondence to:* S. Kim; e-mail: sehkim@hanbit.kaist.ac.kr

Contract/grant sponsor: Korea Science and Engineering

Foundation; contract/grant number: 98-0501-01-01-3

## Introduction

The transition metal clusters have attracted much attention due to their potential applications toward nanoelectronic devices, memory devices, and catalysts.<sup>1–4</sup> An understanding of the thermodynamic properties of small metal clusters as well as their atomic structures has a practical importance in nanoscale materials. Previous experiments<sup>5–8</sup> and theoretical studies<sup>9–14</sup> on melting and freezing for rare gas ( $\text{RG}_N$ ) and metallic ( $\text{M}_N$ ) clusters show that the melting temperatures of small clusters are significantly lower compared to their corresponding bulk, and the melting temperatures are strongly related to their structures. Theoretical studies show that clusters melt over a finite range of temperatures and two-stage melting takes place for the clusters with certain sizes. The multistage melting phenomena have been studied for various types of clusters such as rare gas clusters,<sup>10–14</sup> transition metal clusters,<sup>11</sup> alkali metal clusters,<sup>15</sup> molecular clusters,<sup>16</sup> and bimetallic clusters<sup>17</sup> by molecular dynamics and Monte Carlo simulations.

It is now believed that the capped atoms or vacancies on the icosahedral surface play a crucial role in the low-temperature melting.<sup>18–23</sup> The clusters with adatom on the icosahedral surface such as  $\text{M}_{14}$  and  $\text{M}_{20}$  show two-stage melting based on the heat capacity and the Lindemann index.<sup>21–23</sup> The first stage corresponds to a surface melting associated with the locally destabilized geometrical isomers that resulted from the insertion of the capped atom into the surface layer, and the second stage corresponds to an overall melting.<sup>21–23</sup> Contrary to the case of metallic clusters, two-stage melting has not been reported for the rare gas cluster of  $\text{RG}_{14}$  from the observation of the heat capacity and the Lindemann index curve.<sup>14, 18, 19</sup> The qualitative difference in melting behaviors between metallic clusters and rare gas clusters can be attributed to the difference in the potentials used.<sup>13</sup> Gallego et al.<sup>24, 25</sup> reported that the detailed melting behaviors strongly depend on the size of cluster and the potentials used, and the two-stage melting behavior is a characteristic of the metallic clusters with many body potentials. According to Garzón and Jellinek,<sup>20</sup> the clusters of  $\text{Ni}_{12}$  and  $\text{Au}_{14}$  having one vacancy instead of adatom also show a very low melting temperature, but the distinction between premelting and overall melting based on the heat capacity and the Lindemann index is not possible. Recently, Chen et al.<sup>26</sup> reported that they were able to detect a surface melted phase

prior to overall melting even for the  $\text{Ni}_{13}$  cluster with a perfect icosahedral symmetry. By dividing a cluster into the core and the surface layer, they evaluated the heat capacity and the Lindemann index for each division by Monte Carlo simulation (MC).<sup>26</sup>

The surface-melted phases observed in metallic clusters such as  $\text{M}_{13}$  and  $\text{M}_{14}$  are expected to be different from relatively large clusters because, for these small clusters, the energetic cost required to form the interface may simply be too great to form heterogeneously melted clusters.<sup>10, 11</sup> Even though the method calculating the averaged property for the core and surface atoms, respectively, has been widely used for the studies of the melting of small clusters, it is not sufficient for the elucidation of the detailed melting mechanism by itself.<sup>10, 11, 14, 22, 26</sup> The object of our present work is to develop an analysis technique using the atom-resolved quantities for each atom, and by utilizing this method to investigate temperature-dependent behaviors of three types of  $\text{Ni}_N$  clusters ( $N = 12, 13, 14$ ) in detail.

## Computational Details

We used the standard Metropolis Monte Carlo method for the simulation of melting. In this MC method, each atom is initially moved in three directions by a random walk, and then the energy change for the entire cluster,  $\Delta E$ , associated with the trial movement is calculated. If the energy is lowered, the trial is accepted; otherwise, the trial is accepted with a probability given by a Boltzmann factor  $p = \exp(-\Delta E/k_B T)$ . The acceptance ratio is maintained at about 50% by adjusting the maximum displacement of an atom during the simulation. At each new temperature, the cluster was initially allowed to equilibrate for  $5 \times 10^5$  MC step (MCS) before beginning to record the averaged values of some specific quantities over  $5 \times 10^5$  MCS, where one MCS means sampling all atoms once on the average.

To model the atomic interaction of metallic clusters, the second moment approximation to the tight binding method is employed. The used potential is one of the empirical potentials that can correctly reproduce many basic properties of transition metals in the crystalline and noncrystalline phase, and give good insight into the structures and thermodynamics of the metallic clusters.<sup>20–30</sup> In this potential, the cohesive energy of atom  $i$ ,  $E_c^i$ , is expressed as a sum of two terms, one from the band energy  $E_{\text{band}}^i$  determined by the occupied local density of states, and the other from the repulsive term  $E_{\text{rep}}^i$  determined

by the kinetic energy of electrons and ion core-core interaction.<sup>25, 26</sup> Then the total potential energy of cluster,  $E_t$  can be written as:

$$E_t = \sum_i E_c^i = \sum_i (E_{\text{rep}}^i + E_{\text{band}}^i) \quad (1)$$

$$E_{\text{band}}^i = - \left[ \sum_j \xi_0^2 \exp[-2q(r_{ij}/r_0 - 1)] \right]^{1/2} \\ = -\xi_0 C_i^{1/2} \quad (2)$$

$$E_{\text{rep}}^i = \sum_j A \exp[-p(r_{ij}/r_0 - 1)], \quad (3)$$

where  $C_i$  is an effective coordination number of atom  $i$  and  $r_0$  and  $r_{ij}$  are the nearest-neighbor bond length in a perfect crystal and the distance between atom  $i$  and  $j$ , respectively. The  $A$ ,  $\xi_0$ ,  $p$ , and  $q$  are adjustable parameters that are to be determined by the least-square fitting of the potential energy function to the cohesive energy, lattice constant, and elastic constants of bulk nickel. They are  $A = 0.045787$ ,  $\xi_0 = 1.216867$ ,  $p = 15.128489$ , and  $q = 1.414727$ , respectively. The cutoff distance is taken so that the range is between the third and fourth nearest neighbors. Because the parameters we used are fitted to bulk properties, the degree of their adequacy for clusters with smaller sizes remains an open question. There have been several efforts to produce more adequate potentials for clusters.<sup>27</sup>

To characterize the structural change with temperature, we calculated the effective coordination number  $C_i$  and the root-mean-square fluctuation of the interatomic distances between  $i$ th atom and remaining atoms  $\delta_i$ . These quantities are sensitive to the change of cluster configurations, and represent each atomic state during melting. The  $C_i$ , which is different from the conventional coordination number,<sup>13</sup> is expressed by eq. (4) as follows:

$$\langle C_i \rangle_\tau = \left\langle \sum_j \exp[-2q(r_{ij}/r_0 - 1)] \right\rangle_\tau \quad (4)$$

The  $\delta_i$  is defined as

$$\langle \delta_i \rangle_\tau = \frac{1}{N-1} \sum_{j \neq i}^N \frac{((r_{ij}^2)_\tau - \langle r_{ij}^2 \rangle_\tau)^{1/2}}{\langle r_{ij} \rangle_\tau}, \quad (5)$$

where  $1/(N-1)$  is a normalization factor. Here, the subscript  $\tau$  is the average number of MCS. In addition, the heat capacity has been calculated by using the following formula,

$$C = \frac{\langle E_t^2 \rangle - \langle E_t \rangle^2}{2kT^2}. \quad (6)$$

## Results and Discussion

The structures of metal clusters are obtained by simulated annealing MC method. For  $\text{Ni}_5$ – $\text{Ni}_8$  clusters, the trigonal bipyramid ( $\text{Ni}_5$ ), octahedron ( $\text{Ni}_6$ ), and pentagonal bipyramid ( $\text{Ni}_7$ ), bisdisphenoid ( $\text{Ni}_8$ ), and tricapped trigonal prism ( $\text{Ni}_9$ ) are found to be the most stable structures. The most stable structures of Ni clusters sized from  $N = 10$  to  $N = 30$  are based on icosahedron (IC), where some atoms are added on or removed from the mother cluster of icosahedral  $\text{Ni}_{13}$ ,  $\text{Ni}_{19}$ ,  $\text{Ni}_{23}$ , and  $\text{Ni}_{26}$ . So, the structures of clusters can be classified as the perfect icosahedrons, those of vacancies plus icosahedron, and those of adatoms (or capped atoms) plus icosahedron. The optimized geometries of Ni clusters are the same as those obtained by Doye and Wales using Sutton–Chen potentials<sup>28</sup> and also in good agreement with the results by Depristo et al.<sup>31</sup> using the corrected effective medium (CEM) theory based on the density functional theory. The sequential icosahedral growth of Ni clusters agree with that of gas uptake experiment by Parks et al.<sup>32, 33</sup> The calculated binding energy and the second finite difference of the total energy,  $\Delta_2 E(N) = E(N+1) + E(N-1) - 2E(N)$  are represent in Figure 1. The binding energies in this study agree rather well with the CEM results,<sup>31</sup> but they are slightly low if compared

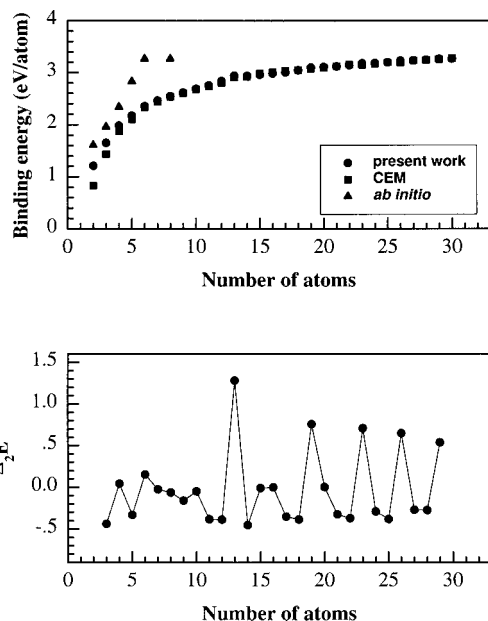


**FIGURE 1.** The binding energies and the  $\Delta_2 E$  are plotted as a function of cluster size. The data of the corrected effective medium (CEM) theory are obtained from ref. 31 and the *ab initio* data from ref. 34.

with the *ab initio* results.<sup>34</sup> The prominent peaks in  $\Delta_2 E(N)$  at  $N = 13, 19, 23, 26$ , and  $29$  imply that 13-, 19-, 23-, 26-, and 29-atom Ni clusters are particularly stable. This result agree well with recent experiments.<sup>32, 33</sup>

Melting temperature of metal clusters have usually been determined by the peak maximum of the heat capacity curve and the incline of the Lindemann index curve.<sup>13, 14, 20–23</sup> However, these two quantities alone are not sufficient to understand the premelting behavior for small metal clusters. Therefore, in this article we examine temperature-dependent behavior of atom-resolved quantities such as  $C_i$  and  $\delta_i$  for  $\text{Ni}_N$  ( $N = 12, 13, 14$ ) clusters as well as the heat capacity and the Lindemann index. Our results prove that atom-resolved quantities are quite useful to understand melting behavior for small clusters. However, for large clusters ( $N > 500$ ), the shell-resolved method can be more effective.<sup>26</sup> Not only the use of diffusivity or pair correlation function but also the shell-resolved Lindemann index or coordination number would be helpful for understanding the melting mechanism of large clusters.

Figure 2 shows the canonical heat capacity for Ni clusters. The heat capacity curves clearly show the broad peak at about 1500 K. This temperature have been accepted as an overall melting temperature

of the cluster. However, the heat capacity curves do not reveal any evidence of two-stage melting. On the other hand, the Lindemann index, which is a nonthermodynamic quantity, clearly shows two-stage melting for  $\text{Ni}_{12}$  and  $\text{Ni}_{14}$  at about 400 K and 1000 K (see Fig. 3). Still, for  $\text{Ni}_{13}$ , any sign of premelting is not observed in the low-temperature region. These results are consistent with the previous reports that the clusters with vacancies and adatoms exhibit lower melting temperatures than the perfect icosahedral cluster, which has rather strong thermal stability.<sup>13, 20, 21</sup> The vacancy and the capped atom on the icosahedral surface are thought to be responsible for the first-stage melting of  $\text{Ni}_{12}$  and  $\text{Ni}_{14}$  clusters, respectively.

To understand the melting behaviors in more detail, the effective coordination numbers for individual atoms,  $\langle C_i \rangle_l$ , are plotted as a function of temperature, as shown in Figure 4, where the numbers in parenthesis represent the number of atoms having the same effective coordination number. The  $\langle C_i \rangle_l$  clearly distinguishes core atoms, surface atoms, and adatoms according to their relative values, because the value for core atoms is the highest and the adatoms and surface atoms have the lowest and intermediate values, respectively. If the configuration of the cluster changes during melting, the  $\langle C_i \rangle_l$  for given atoms will change. For example, if  $i$ th atom

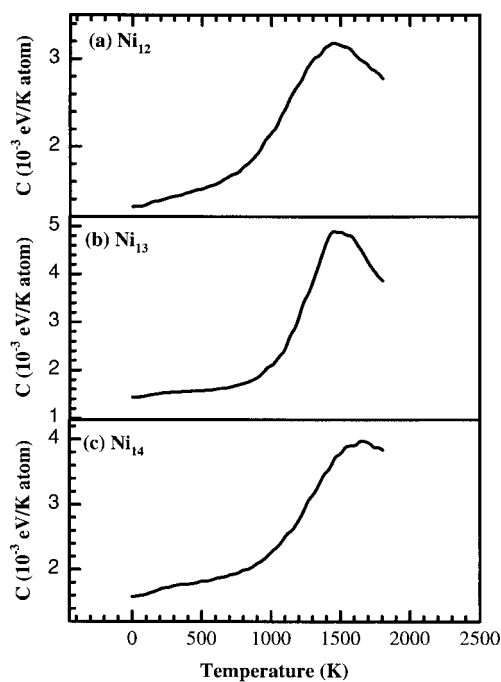


**FIGURE 2.** Heat capacities are plotted as a function of temperature for (a)  $\text{Ni}_{12}$ , (b)  $\text{Ni}_{13}$ , and (c)  $\text{Ni}_{14}$ .

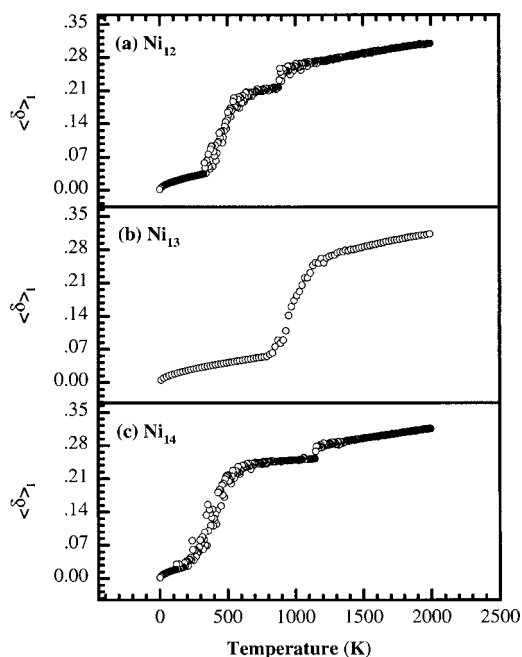


**FIGURE 3.** Lindemann indices  $\langle \delta \rangle_l$  are plotted as a function of temperature, where the number of average  $l$  is  $5 \times 10^5$  MCS for (a)  $\text{Ni}_{12}$ , (b)  $\text{Ni}_{13}$ , and (c)  $\text{Ni}_{14}$ .

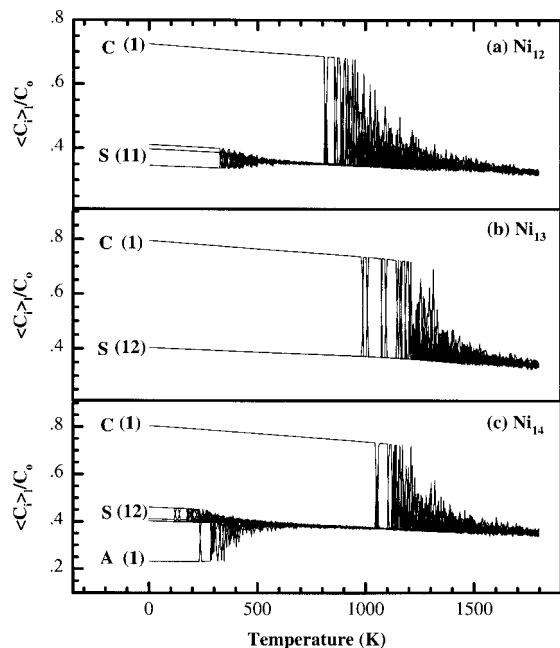


**FIGURE 4.** The effective coordination numbers  $\langle C_i \rangle_l$  of each atom for (a) Ni<sub>12</sub>, (b) Ni<sub>13</sub>, and (c) Ni<sub>14</sub> are plotted for all atoms simultaneously as a function of temperature, where the average number  $l$  at each temperature is  $5 \times 10^5$  MCS. The  $\langle C_i \rangle_l$  values are normalized with  $C_0$ , which is the value of the atom in the bulk crystal in equilibrium state. Text “C,” “S,” and “A” are mean core atoms, surface atoms, and adatoms. The numbers in parenthesis represent the number of atoms having the same effective coordination number.

at the core and  $j$ th atom at the surface exchange their positions, the effective coordination number of  $i$ th will be changed to that of  $j$ th atom and vice versa. At low temperatures (below 200 K), atoms do not exchange their positions. At intermediate temperatures (about 400–500 K), site exchanges among surrounding atoms are observed for Ni<sub>12</sub> and Ni<sub>14</sub>. The Ni<sub>14</sub> cluster shows two types of exchanges at the temperatures of about 300 and 500 K, which will be discussed later. At higher temperatures (800–1200 K), the site exchange between the core atom and surrounding atoms starts to occur. The plot of  $\langle C_i \rangle_l$  for individual atoms clearly shows two- or three-stage melting for Ni<sub>12</sub> and Ni<sub>14</sub>, as shown in Figure 4. The comparison of the  $\langle C_i \rangle_l$  curve with the Lindemann index  $\langle \delta \rangle_l$  curve clearly shows that the low temperature meltings noticed by the rapid increase of the Lindemann index  $\langle \delta \rangle_l$  are due to the site exchange among surrounding atoms, and the high temperature meltings detected by the second abrupt increase of  $\langle \delta \rangle_l$  result from the site exchange between the core atom and surrounding atoms.

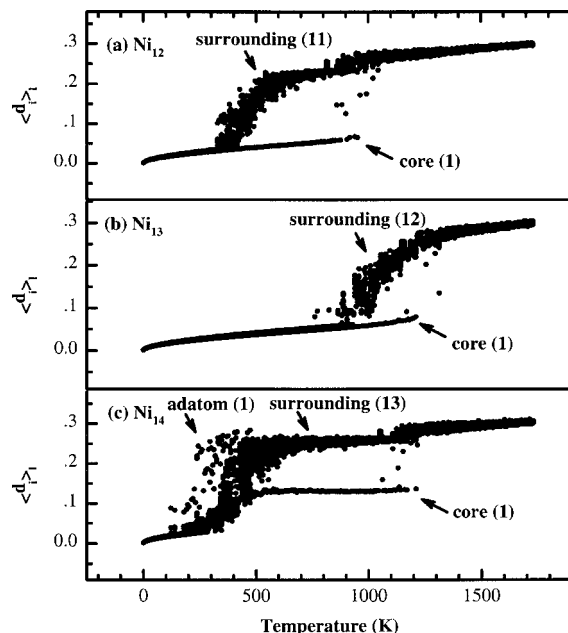


**FIGURE 5.** The rms fluctuation of interatomic distances  $\langle \delta_i \rangle_l$  of each atom (a) Ni<sub>12</sub>, (b) Ni<sub>13</sub>, and (c) Ni<sub>14</sub> are plotted for all atoms simultaneously as a function of temperature, where the average number  $l$  at each temperature is  $5 \times 10^5$  MCS.

The thermal behaviors of individual atoms are studied by the  $\langle \delta_i \rangle_l$ , which measures the extent of melting for individual atoms just as the Lindemann index  $\langle \delta \rangle_l$  measures the extent of melting for the entire cluster. As the temperature increases, a sequence of phase transitions is observed as shown in Figure 5. The splitting of the Lindemann index for surface atoms and core atoms is believed as a direct evidence of surface melting.<sup>11, 14, 22, 26</sup> The plots of  $\langle \delta_i \rangle_l$  show that not only Ni<sub>12</sub> and Ni<sub>14</sub> but also Ni<sub>13</sub> undergo a solid-to-liquid-like transition via the heterogeneously melted phase of solid-like core and liquid-like surrounding, regardless of the existence of a vacancy or an adatom on the icosahedral surface. Here, the heterogeneously melted phase means that the extent of melting is different among atoms. The two-stage melting of Ni<sub>13</sub> is not noticed from  $\langle \delta \rangle_l$  or  $\langle C_i \rangle_l$ . From the study of  $\langle \delta_i \rangle_l$  and  $\langle C_i \rangle_l$ , we can see that the temperature where  $\langle \delta \rangle_l$  changes abruptly and corresponds to the one where the heterogeneously melted phase starts to appear.

To explain the melting behaviors of small clusters with the transient properties of cluster, the technique of averaging a physical quantity for short MCS (or time in MD) has been widely used in the analysis of cluster melting.<sup>13, 18, 19</sup> To interpret the above-mentioned heterogeneous melting with

the isomerization concept, the effective coordination numbers for individual atoms are plotted as a function of MCS at a given temperature, where each point is averaged for short MCS of  $\tau = 500$  (see Fig. 6). This gives information about the instantaneous geometries of clusters because the values of  $\langle C_i \rangle_s$  for individual atoms strongly depend on their local environment in a given structure. For  $\text{Ni}_{12}$ , the  $\langle C_i \rangle_s$  clearly shows that the heterogeneous melting observed from Figure 4(a) and Figure 5(a) is due to the permutational isomerization by the vacancy hopping on the icosahedral surface, which is represented by arrows at several points as shown in Figure 6(a). The two-stage melting behaviors by the vacancy hopping at a low temperature and the site exchange between the core atom and surrounding atoms at a high temperature has not been observed

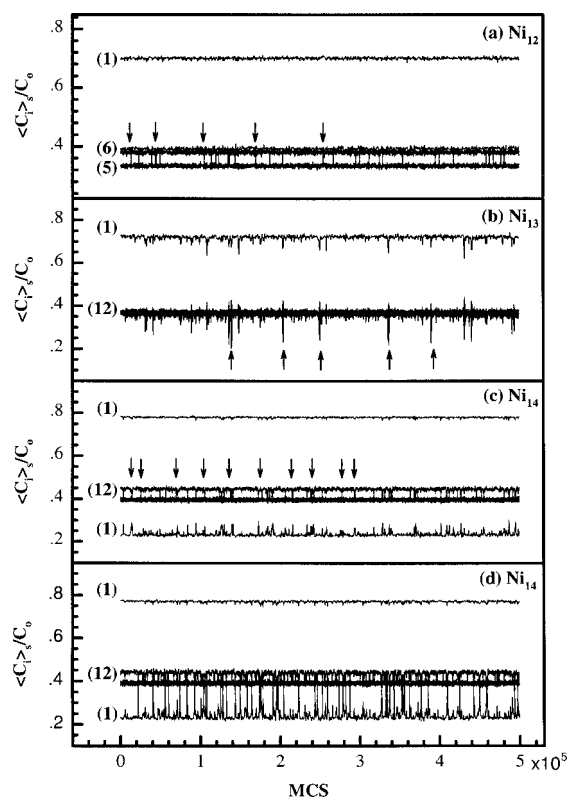


**FIGURE 6.** The  $\langle C_i \rangle_s$  for each atom is plotted as a function of MC trajectory at a fixed temperature. Here, the number of average  $s$  is 500 MCS. The numbers in parenthesis represent the number of atoms having the same effective coordination number, (a)  $\text{Ni}_{12}$  at 400 K. The vacancy hopping is represented by arrows at several points. (b)  $\text{Ni}_{13}$  at 1100 K. The arrows mark the permutational isomerization by the hole-float structure. (c)  $\text{Ni}_{14}$  at 300 K. The adatom hopping is marked by arrows at several points. (d)  $\text{Ni}_{14}$  at 500 K.

either for metallic clusters or for rare gas clusters with the size of  $N < 34$ .<sup>13,14,18–21</sup> For  $\text{Ni}_{13}$ , the  $\langle C_i \rangle_s$  reveals that the heterogeneous melting results from the permutational isomerization via the so-called hole-floater structure. In the hole-floater structure, as marked by the arrow in Figure 6(b), the floater (or adatom) has a much lower value of  $\langle C_i \rangle_s$  than the other surface atoms, and a core atom also has a lower value compared to the one that would be in a perfect icosahedron. This melting mechanism of  $\text{Ni}_{13}$  is quite similar to that of the  $\text{RG}_{13}$  cluster, but the heterogeneously melted phase has not been reported for the  $\text{RG}_{13}$  cluster.<sup>18,19</sup> Chen et al.<sup>26</sup> recently reported that the heterogeneously melted phase appears for  $\text{Ni}_{13}$  in a certain temperature range, but they did not discuss the melting mechanism.

The MCS evolution of  $\langle C_i \rangle_s$  for  $\text{Ni}_{14}$  at about 300 K shows that  $\langle C_i \rangle_s$  for the surface atoms change rapidly between the two marginal values, while the  $\langle C_i \rangle_s$  of adatom is still separated from that of surface atoms (Fig. 6c). This can be explained as the permutational isomerization by the hopping of an adatom on the icosahedral surface. At a higher temperature (500 K), the  $\langle C_i \rangle_s$  shows that the permutational isomerization is accompanied by both the adatom hopping and site exchange between the adatom and the surface atoms (Fig. 6d). Such premelting mechanisms for the  $\text{Ni}_{14}$  cluster are different from the geometrical isomerization mechanisms proposed by Jellinek et al.,<sup>21–23</sup> and it is rather similar to that of the  $\text{RG}_{14}$  cluster.<sup>18,19</sup> Jellinek et al. and Gallego et al. pointed out that the melting behaviors of  $\text{M}_{14}$  clusters depend on the potentials used.<sup>20–25</sup> For example, the  $\text{Ni}_{14}$  cluster exhibits a two-stage melting behavior, while the  $\text{Au}_{14}$  cluster does not.<sup>20–22</sup>

The distribution of potential energy averaged for short MCS can distinguish whether the cluster coexists stochastically (or dynamically in MD) between the geometrical isomers of solid-like and liquid-like clusters or not. The potential energy distributions of  $\text{Ni}_{14}$  shown in Figure 7 exhibit unimodal curves at the temperature region (about 300–1000 K) in which the heterogeneously melted phase appears. The unimodal curve strongly supports that the heterogeneous melting results from the permutational isomerization rather than from the geometrical isomerization. If the heterogeneous melting of  $\text{Ni}_{14}$  were due to the geometrical isomerization between the singly capped icosahedron and the locally melted structures, the potential energy distribution would exhibit a bimodal curve. The potential energy distributions for  $\text{Ni}_{12}$  and  $\text{Ni}_{13}$  clusters also show unimodal curves at the temperatures of heterogeneous melting, which supports that

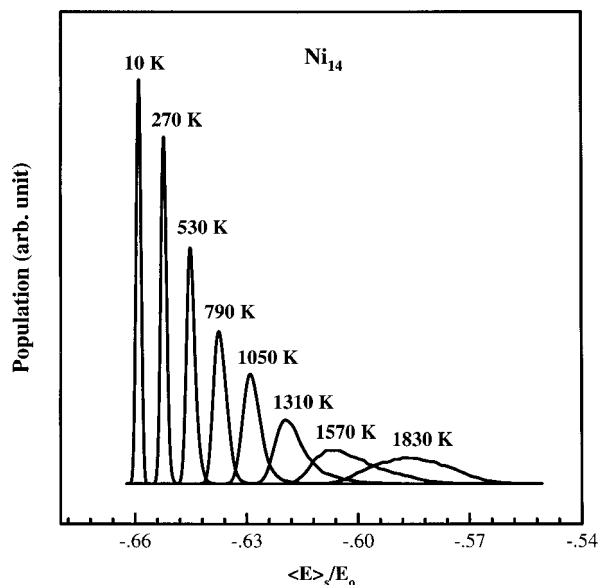


**FIGURE 7.** Probability distributions of potential energy averaged for short time of  $s = 500$  MCS for the  $\text{Ni}_{14}$  cluster. The potential energy is normalized by  $E_0$ , which is the cohesive energy of bulk crystal in equilibrium.

the heterogeneous melted phases of  $\text{Ni}_{12}$  and  $\text{Ni}_{13}$  resulted from permutational isomerization rather than geometrical isomerization.

## Summary

We developed a method that monitors atom-resolved quantities simultaneously for individual atoms as a function of temperature and MCS. The method enables us to clearly explain the temperature-dependent behaviors of small metal clusters. Detailed studies of melting behaviors exhibit the following new results: (a) as the temperature increases, three types of clusters of the icosahedrons with one vacancy, the perfect icosahedrons, and the singly capped icosahedrons show a heterogeneously melted phase prior to overall melting, which implies that the heterogeneous melting is rather intrinsic property of small metal clusters. (b) Based on the atom-resolved technique, it can be concluded that the heterogeneous melting results from the permutational isomerization by the site exchange among surrounding atoms and the overall melting results from the site exchange between the surrounding atoms and the core atom. (c) The melting through the vacancy hopping is observed in icosahedrons with one vacancy. (d) The melting of the singly capped icosahedrons is initiated by the permutational isomerization through

the adatom hopping, followed by the site exchange between the adatom and surface atoms, rather than by the geometrical isomerization between the capped icosahedron and the locally destabilized structures.

## Acknowledgments

We would like to thank Dr. J. Jellinek at Argonne National Laboratory for his kind and helpful discussion. One of us, Y. J. Lee, also thanks Dr. J. P. K. Doye at the University of Cambridge for his helpful discussion on the structures of metal clusters. We are grateful to Mr. Byung Gil Han, Mr. Doo Pyo Lee, and Mr. Byung Tae Jang at the Computer & Software Technology Lab. of Electronics and Telecommunications Research Institute for their permission to use the supercomputer and workstations.

## References

1. Sugano, S.; Nishina, Y.; Ohnishi, S. *Microclusters: Proceedings of the First NEC Symposium*; Springer Verlag: New York, 1987.
2. Haberland, H. *Clusters of Atoms and Molecules I: Theory, Experiment, and Clusters of Atoms*; Springer Verlag: New York, 1995.
3. Martin, T. P. *Large Clusters of Atoms and Molecules*; Kluwer Academic: Boston, 1995.
4. Jena, P.; Khanna, S. N.; Rao, B. K. *Proceedings of the Science and Technology of Atomically Engineered Materials*; World Scientific: NJ, 1995.
5. Buffat, Ph.; Borel, J.-P. *Phys Rev A* 1976, 13, 2287.
6. Lai, S. L.; Guo, J. Y.; Petrova, V.; Ramanath, G.; Allen, L. H. *Phys Rev Lett* 1996, 77, 99.
7. Schmidt, M.; Kusche, R.; Kronmüller, W.; von Issendorff, B.; Haberland, H. *Phys Rev Lett* 1997, 79, 99.
8. Peters, K. F.; Cohen, J. B.; Chung, Y.-W. *Phys Rev B* 1998, 57, 13430.
9. Rytönen, A.; Häkkinen, H.; Manninen, M. *Phys Rev Lett* 1998, 80, 3940.
10. Cheng, H.-P.; Berry, R. S. *Phys Rev A* 1992, 45, 7969.
11. Güvenç, Z. B.; Jellinek, J. *Z Phys D* 1993, 26, 304.
12. Ercolessi, F.; Andreoni, W.; Tosatti, E. *Phys Rev Lett* 1991, 66, 911.
13. Vlachos, D. G.; Schmidt, L. D.; Aris, R. *J Chem Phys* 1992, 96, 6891.
14. Calvo, F.; Labatie, P. *Chem Phys Lett* 1996, 258, 233.
15. Calvo, F.; Spiegelmann, F. *Phys Rev Lett* 1999, 82, 2270.
16. Maillat, J.-B.; Boutin, A.; Fuchs, A. H. *Phys Rev Lett* 1996, 76, 4336.
17. López, M. J.; Marcos, P. A.; Alonso, J. A. *J Chem Phys* 1996, 104, 1056.
18. Doye, J. P. K.; Wales, D. J. *J Chem Phys* 1995, 102, 9673.

19. Beck, T. L.; Jellinek, J.; Berry, R. S. *J Chem Phys* 1987, 87, 545.
20. Garzón, I. L.; Jellinek, J. *Z Phys D* 1993, 26, 316.
21. Jellinek, J.; Garzón, I. L. *Z Phys D* 1993, 20, 239.
22. Jellinek, J.; Güvenç, Z. B. In *The Synergy Between Dynamics and Reactivity at Clusters and Surfaces*; Farrugia, L. J., Ed.; Academic: The Netherlands, 1995, p. 217.
23. Garzón, I. L.; Jellinek, J. In *Physics and Chemistry of Finite systems: From Clusters to Crystals*; Jena, P.; Khanna, S. N.; Rao, B. K., Eds.; Academic: The Netherlands, 1992, p. 405, vol. 1.
24. Garcia-Rodeja, J.; Rey, C.; Gallego, L. J.; Alonso, J. A. *Phys Rev B* 1994, 49, 8495.
25. Rey, C.; Gallego, L. J.; Garcia-Rodeja, J.; Alonso, J. A.; Iñiguez, M. P. *Phys Rev B* 1993, 48, 8253.
26. Chen, X.; Zhao, J.; Sun, Q.; Liu, F.; Wang, G.; Shen, X. C. *Phys Stat Sol* 1996, 193, 355.
27. López, M. J.; Jellinek, J. *J Chem Phys* 1999, 110, 8899; and references therein.
28. Doye, J. P. K.; Wales, D. J. *New J Chem* 1998, 22, 733.
29. Granja, F. A.; Bouarab, S.; López, M. J.; Vega, A.; Carrizales, J. M. M. *Phys Rev B* 1998, 57, 12469.
30. Carrizales, J. M. M.; Iñiguez, M. P.; Alonso, J. A.; López, M. J. *J Phys Rev B* 1996, 54, 5961.
31. Stave, M. S.; DePristo, A. E. *J Chem Phys* 1992, 97, 3386.
32. Parks, E. K.; Zhu, L.; Ho, J.; Riley, S. J. *J Chem Phys* 1994, 100, 7206.
33. Parks, E. K.; Zhu, L.; Ho, J.; Riley, S. J. *J Chem Phys* 1995, 102, 7377.
34. Reuse, F. A.; Khanna, S. N. *Chem Phys Lett* 1995, 234, 77.